Power Electronic Systems
Laboratory

Proceedings of the 7th IEEE Southern Power Electronics Conference (IEEE SPEC 2022), Fiji, December 5-8, 2022

New Concept for Current-Impressed WPT to Multiple Independent Stainless-Steel-Enclosed Linear Actuator Sliders

P. Jayathurathnage,
S. Miric,
J. Xu,
J. Huber,
M. Hitz,
J. Kyyrä,
J. W. Kolar

Eidgenössische Technische Hochschule Zürich
Swiss Federal Institute of Technology Zurich

New Concept for Current-Impressed WPT to Multiple Independent Stainless-Steel-Enclosed Linear Actuator Sliders

Prasad Jayathurathnage[1,2], Spasoje Mirić[1], Junzhong Xu[1], Jonas Huber[1], Marco Hitz[3], Jorma Kyyrä[2], Johann W. Kolar[1]

[1]Power Electronic Systems Laboratory, ETH Zurich, Zurich, Switzerland
[2]School of Electrical and Electronics Engineering, Aalto University, Finland
[3]NTI AG, Spreitenbach, Switzerland

***Abstract*—Linear actuators (LAs) in pharmaceutical or chemical industries must be encapsulated into stainless steel (SS) enclosures to comply with extreme purity standards and facilitate thorough cleaning and disinfection. Therefore, advantageously wireless power transfer (WPT) should be used to supply the sliding part of such actuators, with the primary winding extended to cover the entire LA stroke, such that hard-to-clean cable carrier assemblies can be eliminated. Typically multiple independent sliders and/or tool carriages must then be supplied from the same primary winding, resulting in a multi-receiver WPT system. However, providing power with a voltage-impressed method to such a system is challenging due to the voltage sharing among the receivers. Therefore, this paper proposes a novel current-impressed method suitable for multi-receiver WPT systems. The proposed method is thoroughly analyzed, optimized, verified by circuit simulations, and compared against a conventional current-impressed approach. As a result, the proposed method facilitates overload capability and has higher efficiency. The exemplary system is designed for two 100 W tool carriages and 72 V DC input and output voltages.**

I. Introduction

Linear actuators (LAs) are electrical machines used in various high-end industrial systems to perform positioning tasks, e.g., in semiconductor or electronics manufacturing industries for pick-and-place robots or pharmaceutical and chemical industries for automating various processes. Typically, such industries have extreme hygiene standards which they can only meet if the used equipment is encapsulated in stainless steel (SS) enclosures, typically built out of SS sheets. Furthermore, supplying power to the slider/moving parts (tool carriages, etc.) of LAs requires moving cables and cable carriers, which are exposed to tear and wear due to the typically highly repetitive operation of LAs (e.g., high acceleration pick-and-place robots move up to 10000 times per hour). Consequently, they contaminate the environment and are challenging to clean, increasing the downtime for washing and the maintenance cost. In addition, the moving cables often require change as they have a limited lifetime; they attenuate the LA's dynamics due to their mass and are typically not shielded to minimize the weight, so complying with EMI standards is an additional challenge. Alternatively, wireless power transfer (WPT) to the moving sliders and tool carriages of the LA allows to eliminate the cables and cable carriers [1]–[8].

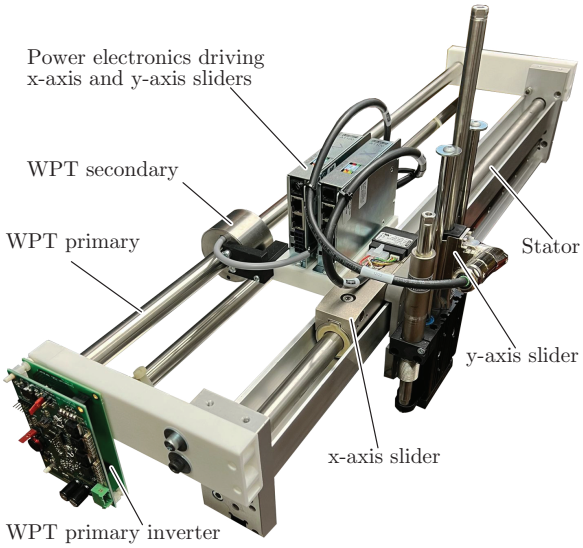

Fig. 1: Stainless-steel-(SS)-enclosed linear actuator with WPT to a single moving slider that integrates the LA (linear motor) windings and carries the power electronics converter impressing the winding currents according to the desired slider movement. (Note that the stationary tube-shaped LA part contains a stack of alternately magnetized permanent magnets [9], [10].)

Nevertheless, conventional WPT systems for LAs can not be directly applied to the actuators enclosed in SS; the WPT's coupling magnetic field would cause eddy current losses in SS sheets and severely deteriorate efficiency [11]. Therefore, in recent literature [12] (cf. **Fig. 1**), an enclosure method of the WPT into the SS sheets is proposed where the high WPT efficiency is kept (97 % at 100 W, 72 V). The concept is depicted in **Fig. 2**), based on a coaxial arrangement of the primary and the secondary, where the coupling flux lines are circular and tangential to the SS sheets. Consequently, the low thickness of the SS sheets limits the cross-section where eddy currents can be induced, similar to laminations

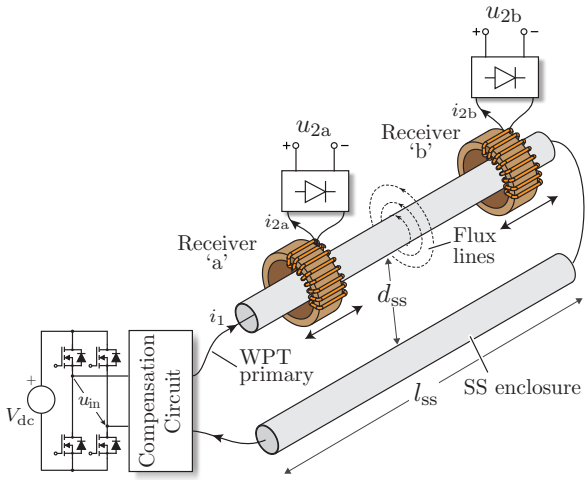

Fig. 2: Schematic illustration of a WPT system with two sliders/receivers; depending on the excitation type (voltage-impressed or current-impressed), different compensation circuits are used, cf. **Fig. 3**.

of the magnetic core of power transformers. Therefore, the coaxial arrangement makes the SS enclosure magnetically "transparent," and its impact on the WPT efficiency can be neglected [12].

It can be seen in **Fig. 1** that the primary winding, enclosed in the SS tube, has a length that covers the total linear stroke of the actuator. To increase the throughput of, e.g., pick-and-place robots, LAs are frequently equipped with multiple independent sliders which are supplied from the same primary winding, resulting in multiple-receiver WPT, as shown in **Fig. 2** for two sliders/receivers. However, as discussed in [12], the multi-receiver WPT equivalent circuit is equivalent to a series connection of the loads. Therefore, supplying the loads in such cases can be very challenging because the voltages are shared between the loads in the case of the voltage-impressed WPT supply, as shown in [12]. In addition, the output powers of the two loads are coupled, e.g., if one load draws zero power, the rest of the loads cannot receive any power. Therefore, so-called voltage sharing can be implemented, where only a single load is connected to the primary at any point in time.

The other loads are disconnected by short-circuiting the rectifier on the secondary side. Like this, the issues with the voltage sharing and the power coupling between the loads can be solved, cf. [12]. Nevertheless, this approach increases the system's complexity, where active rectifier stages must be used (see **Fig. 3(a)**). Moreover, to ensure a suitable moment of switching between the loads, synchronization between the loads must exist.

Alternatively, current-impressed methods, where the primary current amplitude is kept constant regardless of the load or the number of loads, have been proposed to implement multi-receiver WPT systems [13]–[15]. **Fig. 3(b)** shows a conventional, current-impressed two-receiver WPT system. As shown in the phasor diagram, which will be explained in detail later in the paper, the core flux density depends on the load current, which is not desirable when the slider of a LA is supplied due to the high overloads typical for its operation. Therefore, we propose a new current-impressed WPT shown in **Fig. 3(c)**, where the dependency of the core flux density on the load current is attenuated by phase shifting the load current, which is achieved by removing the series-resonant compensation capacitors (C_{2a} and C_{2b}). Nevertheless, this requires active rectifiers to control the output voltages (U_{outa} and U_{outb}), but no synchronization between the loads is necessary, like for the voltage-impressed WPT systems. Hence, the proposed method can also be used with more than two receivers without increased complexity or control, which substantially differs from the voltage-impressed WPT, where voltage sharing must be implemented.

TABLE I: System specifications considering two sliders/receivers a and b.

Parameter	Symbol	Value	Unit
DC input voltage	U_{dc}	72	V
DC output voltage	$U_{out\{a,b\}}$	72	V
Output power (per receiver)	$P_{out\{a,b\}}$	100	W
Length of SS pipe	l_{ss}	118	cm
Distance between SS pipes	d_{ss}	10	cm

Therefore, this paper summarizes the advantages and drawbacks of the supply methods for multi-receiver WPT systems and compares the conventional and the proposed current-impressed methods, cf. **Sec. II**. In **Sec. III**, we design and optimize the current-impressed methods and compare them for their efficiency versus output power. **Sec. IV** concludes the paper.

II. Multi-Receiver WPT Supply Options

This paper considers the exemplary case of two LA sliders/receivers, as shown in **Fig. 2**, where the receivers are modeled using a transformer equivalent circuit. The voltage-impressed WPT scheme is illustrated in **Fig. 3(a)**, while the conventional current-impressed approach and the proposed current-impressed approach are presented in **Fig. 3(b,c)**. The primary winding leads through the SS enclosure and/or stationary SS tubes and the toroidal magnetic cores. For modeling purposes, the self-inductance of the primary is represented in three components, inductance resulting from the segments of two receiver cores L_{1a} and L_{1b}, and the rest of the primary loop inductance L_1, where the total inductance of the primary is $L_{1a}+L_{1b}+L_1$. The secondary self-inductance L_{2a} and L_{2b}, and mutual inductance between primary and secondary M_a and M_b, are used to model the transformer. Primary winding and SS losses are modeled with a series resistor R_1 [12]. This section discusses the WPT approaches shown in **Fig. 3**. The specification of the analyzed two-receiver WPT system is given in **Tab. I**.

A. Voltage-Impressed WPT

The voltage-impressed WPT scheme is shown in **Fig. 3(a)** and employs the series-resonant "DC transformer" (DCX) converter [12], [16], where the primary leakage inductance of

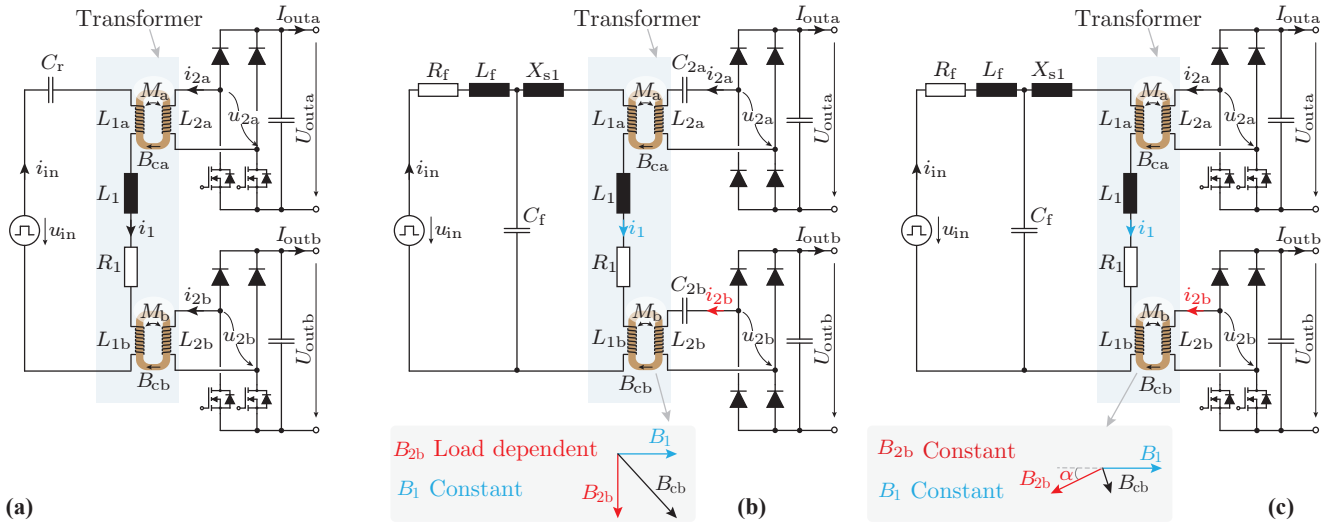

Fig. 3: Power circuits of the analyzed options for WPT to multiple receivers (two shown as an exemplary case). The input voltage u_{in} is the output voltage of the primary-side full-bridge inverter shown in **Fig. 2**, and $u_{2\{\text{a,b}\}}$ is the input voltage of the rectifiers of the receivers/slides a and b (U_{in} and $U_{2\{\text{a,b}\}}$ denote the fundamental frequency component of u_{in} and $u_{2\{\text{a,b}\}}$, respectively). R_1 models the total series resistance of the stretched-out, long primary winding. **(a)** Voltage-impressed system where C_{r} is the compensation circuit. **(b)** Conventional and **(c)** proposed new current-impressed systems, where R_{f}, L_{f}, C_{f} and X_{s1} form the compensation circuit. Note that the conventional variant also requires a compensating capacitor ($C_{2\{\text{a,b}\}}$) on the secondary side.

the WPT transformers is compensated using a series capacitor C_{r}. The configuration impresses a voltage on the primary side; thus, the total secondary voltage is also impressed. Here, the primary and secondary work as a classical transformer where the primary and secondary currents mostly compensate each other. Hence, the core flux density depends only on the applied voltage-time area on the primary, not the load. Furthermore, given the magnetic series connection of the secondaries, only one receiver should be active at any given time; otherwise, if multiple secondaries are engaged, the total voltage is shared among the receivers, resulting in decreased output voltages. Therefore, a time-sharing operation method is proposed in [12], where the two receivers switch the power reception periodically, i.e., always one receiver short-circuits its secondary winding at a time. This approach requires synchronization of the receivers and employment of non-conventional state-machine-based control of the voltage and power sharing. It becomes more challenging with more than two receivers as the complexity of voltage sharing increases.

B. Conventional Current-Impressed WPT

The current-impressed WPT that ensures a constant current in the primary winding is widely used for multi-receiver WPT [17]. For example, as illustrated in **Fig. 4**, the insertion of a symmetric T-network with reactances $\text{j}X$ in the series and $-\text{j}X$ in the parallel branch impresses a current $I_1 = U_{\text{in}}/\text{j}X$ in the load impedance Z_{T}. In principle, the reactance X can either be positive or negative, which is realized using inductive or capacitive components.

Therefore, implementation of the T-network for the two-receiver WPT system is shown in **Fig. 3(b)**, where $X = \omega L_{\text{f}}$ realizes a load-independent constant current $I_1 = U_{\text{in}}/\text{j}\omega L_{\text{f}}$ in

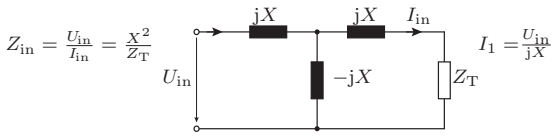

Fig. 4: Symmetric T-network that converts a voltage-impressed load into a current-impressed load, i.e., the load current I_1 does not depend on the load impedance Z_{T}.

the primary winding with an additional compensation circuit consisting of L_{f}[1], C_{f} and X_{s1} [13], [14]. The choice of these elements assumes that the transformer parameters, L_1, $L_{1\text{a}}$, $L_{2\text{a}}$, M_{a}, $L_{1\text{b}}$, $L_{2\text{b}}$ and M_{b} are known. The design process of the conventional current-impressed WPT scheme starts with tuning the secondary compensation capacitors $C_{2\{\text{a,b}\}}$ to fully compensate secondary inductances $L_{2\{\text{a,b}\}}$, i.e.,

$$C_{2\{\text{a,b}\}} = \frac{1}{\omega^2 L_{2\{\text{a,b}\}}}. \tag{1}$$

As the secondary loop is fully compensated, the fundamental component of the ac output voltage becomes

$$U_{2\{\text{a,b}\}} = \text{j}\omega M_{\{\text{a,b}\}} I_1 = M_{\{\text{a,b}\}} U_{\text{in}}/L_{\text{f}}.$$

With the assumption of identical secondary windings (i.e. $M_{\text{a}} = M_{\text{b}} = M$), the voltage gain becomes

$$G_{\text{v}\{\text{a,b}\}} = \frac{U_{2\{\text{a,b}\}}}{U_{\text{in}}} = \frac{M}{L_{\text{f}}}, \tag{2}$$

that determines the first parameter in the primary compen-

[1]Note that R_{f} is the resistance of the inductor L_{f}, and its value should be minimized.

sation network L_f, which is set so the desired voltage gain is achieved. In this paper, $G_{\mathrm{v}\{\mathrm{a,b}\}} = 1$, which leads to $L_\mathrm{f} = M/G_{\mathrm{v}\{\mathrm{a,b}\}} = M$. Next, parallel capacitor C_f is tuned to resonate with L_f at switching frequency as

$$C_\mathrm{f} = \frac{1}{\omega^2 L_\mathrm{f}}. \tag{3}$$

Finally, the value of X_{s1} is calculated to provide the difference of the reactance of primary inductance and required reactance $\mathrm{j}X$ so that the input impedance at the output of the full-bridge converter becomes resistive as

$$X_{\mathrm{s1}} = \omega L_\mathrm{f} - \omega(L_1 + L_{1\mathrm{a}} + L_{1\mathrm{b}}). \tag{4}$$

The reactance X_{s1} is externally added using an inductor, if $X_{\mathrm{s1}} > 0$, or a capacitor if $X_{\mathrm{s1}} < 0$.

As load-independent secondary voltages are realized, communication and synchronization between multiple receivers are unnecessary. However, in contrast to typical WPT applications (with typically significant air gaps), the SS application requires a closed magnetic core for each receiver to minimize the stray fields that induce eddy current losses in the SS enclosures. Therefore, the magnetic flux density of the core needs to be carefully analyzed to ensure the operation of the core within the saturation limits. In the conventional current-impressed WPT, the induced voltage on the secondary current

$$I_{2\{\mathrm{a,b}\}} = \mathrm{j}\left(\frac{-\omega M}{R_{\mathrm{eq}\{\mathrm{a,b}\}}}\right) I_1 \tag{5}$$

that is orthogonal to I_1 in phasor representation where $R_{\mathrm{eq}\{\mathrm{a,b}\}} = 8U_{\mathrm{out}\{\mathrm{a,b}\}}/\pi^2 I_{\mathrm{out}\{\mathrm{a,b}\}}$ represents the equivalent ac load at the input terminals of the rectifier (cf. **Fig. 3**). The equivalent ac load $R_{\mathrm{eq}\{\mathrm{a,b}\}}$ and the secondary current $I_{2\{\mathrm{a,b}\}}$ vary with the change in load power.

The magnetic flux density in the core $B_{\mathrm{c}\{\mathrm{a,b}\}}$ (in phasor form, cf. **Fig. 3(b,c)**) can be calculated as

$$B_{\mathrm{c}\{\mathrm{a,b}\}} = \frac{\mu}{l_\mathrm{e}}\left(N_1 I_1 + N_2 I_{2\{\mathrm{a,b}\}}\right), \tag{6}$$

where μ is the permeability of the core and l_e is the effective magnetic length of the core. The flux components generated by the primary and the secondary winding are perpendicular in phasor representation (cf. inset in **Fig. 3(b)**). As the secondary current $I_{2\{\mathrm{a,b}\}}$ is load dependent, this results in a load-dependent magnetic flux density $B_{\mathrm{c}\{\mathrm{a,b}\}}$ in the closed core which increases with the increase of the load power. Thus, in the case of, e.g., short-term overloads that typically can occur during LA acceleration phases, the correspondingly increasing secondary winding current can drive the core into saturation (cf. also **Fig. 3(b)**). In addition, it can be observed from (6) that the core flux density is proportional to the effective permeability of the core. In the case of typical current impressed WPT applications, there is a large air gap between the primary and the secondary, which makes the effective permeability very small. However, in our proposal, we need to have closed magnetic cores to ensure lower SS losses, hence high permeability of the core material may lead to higher magnetic flux densities. Therefore, the main limitation of this conventional current-impressed method for WPT with closed magnetic cores originates from the risk of core saturation at higher power.

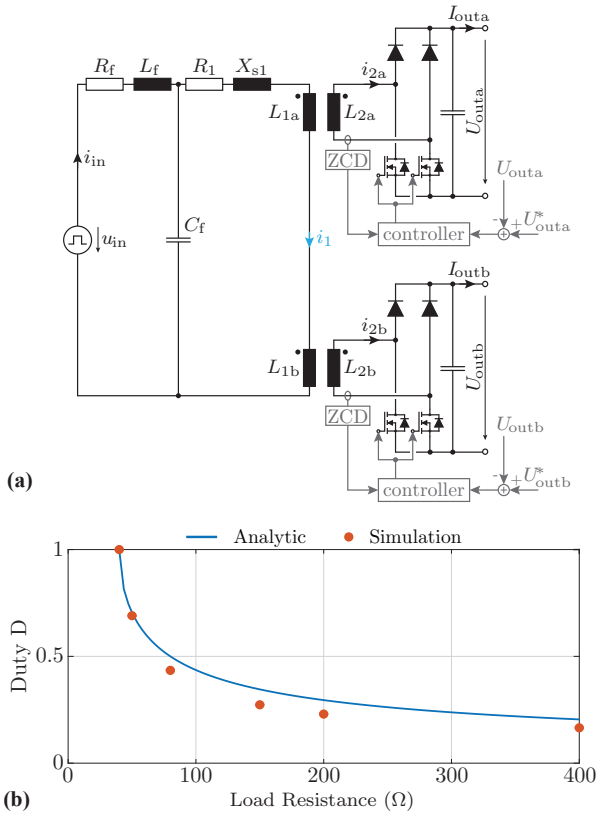

Fig. 5: (a) Voltage control scheme of the proposed current-impressed WPT scheme. **(b)** Duty cycle of the active rectifier with respect to load resistance R_load to keep constant load voltage ($U_\mathrm{out} = 72\,\mathrm{V}$).

C. Proposed Current-Impressed WPT

To eliminate this drawback of the conventional current-impressed WPT, we propose a new modified current-impressed topology as depicted in **Fig. 3(c)**. Here, the secondary loop inductance is not compensated, i.e., no series capacitor exists. On the other hand, the compensation network on the primary side still ensures a current-impressed primary winding as $I_1 = U_\mathrm{in}/\mathrm{j}\omega L_\mathrm{f}$. Hence, the two receivers work independently without cross-interaction; i.e., the power variation in one receiver does not affect the voltage of the other receiver. With this configuration, the secondary current becomes

$$I_{2\{\mathrm{a,b}\}} = \frac{-\mathrm{j}\omega M_{\{\mathrm{a,b}\}}}{R_{\mathrm{eq}\{\mathrm{a,b}\}} + \mathrm{j}\omega L_{2\{\mathrm{a,b}\}}} I_1, \tag{7}$$

which makes an angle $(\pi + \alpha)$ where $\alpha = \tan^{-1}(R_\mathrm{eq}/\omega L_2)$ with respect to the primary current I_1. In order to minimize the magnetizing current, the goal is to make the phase angle between I_1 and $I_{2\{\mathrm{a,b}\}}$ close to π, i.e., to minimize α as much as possible. Angle α can be minimized by increasing $L_{2\{\mathrm{a,b}\}}$ and decreasing $R_{\mathrm{eq}\{\mathrm{a,b}\}}$. However, if $R_{\mathrm{eq}\{\mathrm{a,b}\}}$ is substantially smaller than the reactance of the secondary winding $\omega L_{2\{\mathrm{a,b}\}}$,

there will be a higher voltage drop across the secondary winding. Therefore, with proper optimization of secondary inductance $L_{2\{\mathrm{a,b}\}}$ (i.e., by optimization of secondary turns, core dimensions, and core material), and equivalent load resistance $R_{\mathrm{eq}\{\mathrm{a,b}\}}$, the magnetic field created by the secondary winding current (partly) compensates the field created by the primary current, as illustrated in the phasor diagram in **Fig. 3(c)**.

The design steps of the proposed current-impressed WPT scheme are discussed to elaborate the working principle. The component values of the compensation circuit are designed by considering the nominal operation at the rated power. First, it is assumed that two receiver windings are identical (i.e., $L_{2\mathrm{a}} = L_{2\mathrm{b}} = L_2$ and $M_{\mathrm{a}} = M_{\mathrm{b}} = M$), and the rated power of both loads is the same, which leads to identical equivalent loads at the nominal power (i.e. $R_{\mathrm{eqN}} = R_{\mathrm{eq}\{\mathrm{a,b}\}}$ at the nominal power). The value of the compensation inductor L_{f} is determined by the desired voltage gain at the nominal load (i.e., $G_{\mathrm{vN}} = U_{2\{\mathrm{a,b}\}}/U_{\mathrm{in}}$) of the system as

$$L_{\mathrm{f}} = \frac{M R_{\mathrm{eqN}}}{G_{\mathrm{vN}}\sqrt{R_{\mathrm{eqN}}^2 + \omega^2 L_2^2}}, \tag{8}$$

where $I_1 = U_{\mathrm{in}}/\mathrm{j}\omega L_{\mathrm{f}}$ and $I_{2\{\mathrm{a,b}\}} = U_{2\{\mathrm{a,b}\}}/R_{\mathrm{eqN}}$ are replaced into (7) and later solved for L_{f}. Next, similar to the conventional current impressed WPT, parallel capacitor C_{f} is tuned to resonance with front-end inductor L_{f} at the switching frequency as $C_{\mathrm{f}} = 1/\omega^2 L_{\mathrm{f}}$. The series reactance X_{s1} connected to the primary is tuned to have resistive input impedance at the nominal load as

$$X_{\mathrm{s1}} = \omega L_{\mathrm{f}} - \omega(L_1 + L_{1\mathrm{a}} + L_{1\mathrm{b}}) + \frac{n_{\mathrm{rec}}\omega^3 L_2 M^2}{R_{\mathrm{eqN}}^2 + \omega^2 L_2^2}, \tag{9}$$

where n_{rec} is the number of receivers and $n_{\mathrm{rec}} = 2$ for the system considered in this paper. The required reactance X_{s1} is realized either by using an inductor (if $X_{\mathrm{s1}} > 0$) or a capacitor (if $X_{\mathrm{s1}} < 0$).

As the compensation circuit is tuned at the nominal load, it is important to investigate the characteristics at an arbitrary load. The voltage gain $G_{\mathrm{v}\{\mathrm{a,b}\}}$ at an arbitrary equivalent ac load $R_{\mathrm{eq}\{\mathrm{a,b}\}}$ reads

$$G_{\mathrm{v}\{\mathrm{a,b}\}} = G_{\mathrm{vN}}\frac{R_{\mathrm{eq}\{\mathrm{a,b}\}}}{R_{\mathrm{eqN}}}\sqrt{\frac{R_{\mathrm{eqN}}^2 + \omega^2 L_2^2}{{R_{\mathrm{eq}\{\mathrm{a,b}\}}}^2 + \omega^2 L_2^2}}. \tag{10}$$

It is clear from (10) that the proposed topology yields a load dependency on the receivers' output voltages, as such, output voltage regulation needs to be implemented. Therefore, the key idea of the proposed concept is to keep $R_{\mathrm{eq}\{a,b\}}$ constant. As illustrated in **Fig. 5(a)**, an active rectifier control can be easily implemented with the receiver [18]. The control scheme still operates self-contained without communication or synchronization between multiple receivers, simplifying the practical implementation. The duty cycle of the active rectifier $D_{\{\mathrm{a,b}\}}$ at a given dc load $R_{\mathrm{load}\{\mathrm{a,b}\}} = U_{\mathrm{out}\{\mathrm{a,b}\}}/i_{\mathrm{out}\{\mathrm{a,b}\}}$ and fixed output voltage $U_{\mathrm{out}\{\mathrm{a,b}\}}$ depends on the nominal load at the rated power R_{loadN} and the duty cycle at the nominal load D_{N} as

$$D_{\{\mathrm{a,b}\}} = \frac{2}{\pi}\cos^{-1}\left(1 - \frac{R_{\mathrm{loadN}}}{R_{\mathrm{load}\{\mathrm{a,b}\}}}\sin^2\left(\frac{D_{\mathrm{N}}\pi}{2}\right)\right). \tag{11}$$

The variation of $D_{\{\mathrm{a,b}\}}$ against the load resistance is shown in **Fig. 5(b)**. At the nominal load, the active rectifier operates in full-wave rectification mode with $D_{\mathrm{N}} = 1$, and $D_{\{\mathrm{a,b}\}} < 1$ for partial loads to ensure voltage regulation at the output. To further elaborate the working principle of the proposed method with active rectifier control, **Fig. 6** shows the simulated waveforms at the nominal load and $10\,\%$ load for one receiver. The continuous control of $D_{\{\mathrm{a,b}\}}$ ensuring a constant output voltage results in a constant equivalent load resistance

$$R_{\mathrm{eq}\{\mathrm{a,b}\}} = \frac{8}{\pi^2}R_{\mathrm{loadN}}\sin^2(\frac{\pi D_{\mathrm{N}}}{2}), \tag{12}$$

Therefore, the secondary current is also impressed at

$$I_{2\{\mathrm{a,b}\}} = \frac{-\mathrm{j}\omega M}{\mathrm{j}\omega L_2 + 8R_{\mathrm{loadN}}\sin^2(\pi D_{\mathrm{N}}/2)/\pi^2}I_1. \tag{13}$$

It can be noticed from the simulation waveform in **Fig. 6** that primary and secondary current are almost constant for both $100\,\%$ and $10\,\%$ loads. The angle α between primary and secondary currents becomes

$$\alpha = \tan^{-1}\left(\frac{8R_{\mathrm{loadN}}\sin^2(\pi D_{\mathrm{N}}/2)}{\pi^2\omega L_2}\right). \tag{14}$$

As the primary and secondary currents are load-independent, the fundamental component of the magnetizing current is load-independent, which differs from the conventional current-impressed method, where the magnetizing current is load-dependent. Taking the analogy of traditional transformer characteristics in the voltage-impressed WPT approach, we have current-impressed primary and secondary, where both methods have load-independent low magnetizing current. As a result, the latter has the advantage of independent operation of multiple receivers without cross-interaction. However, load-independent currents may lead to lower efficiency at light load conditions.

As the proposed scheme is designed to have a maximum duty cycle at the nominal load (i.e., $D_{\mathrm{N}} = 1$), if an overload happens (i.e., R_{load} goes below R_{loadN}) the output voltage will be decreased from its nominal value (cf. (10)). Therefore, if an overload condition exceeds the designed nominal design power, which implies natural overload protection. In case the number of receivers is increased with the exact per-load specifications, the value of reactance X_{s1} needs to be redesigned to compensate for the reactive impedance brought by the additional receivers (cf. (9)), however, the rest of the component values remain unchanged.

III. Design Optimization and Comparative Evaluation

A. Design Optimization

This section presents a case study comparing the conventional current-impressed method and the proposed current-

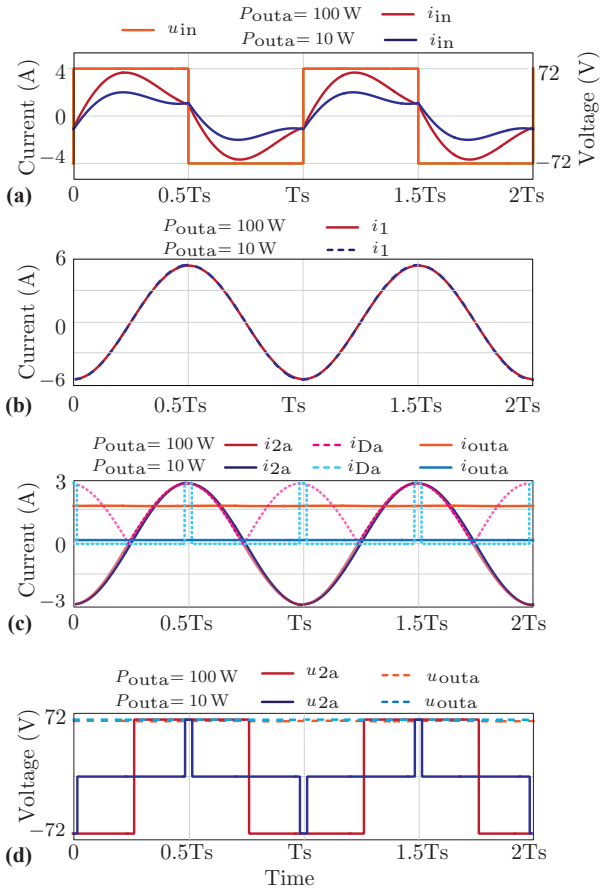

Fig. 6: Simulated key waveforms of the proposed current-impressed WPT system from **Fig. 3(c)** for two power levels (i.e., 100 W and 10 W) of one load (load "a") while the second load (load "b") is working at full power (i.e., 100 W).

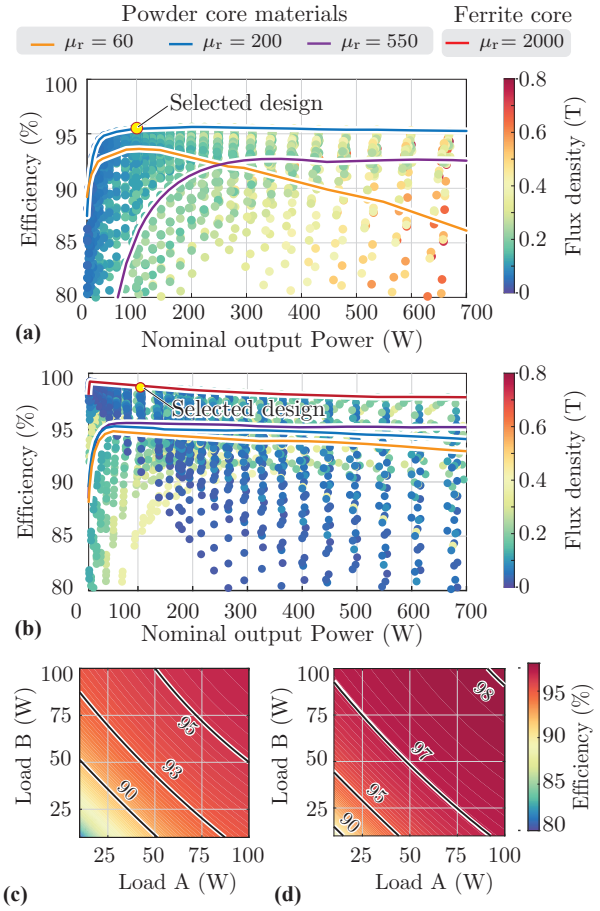

Fig. 7: (a,b) Optimized efficiency of the WPT system against per load power with different core types: **(a)** conventional current-impressed WPT system, and **(b)** proposed current-impressed WPT system. Scatter plots refer to the possible design points for the core material with the highest efficiency i.e., $\mu_r = 200$ for **(a)**, and $\mu_r = 2000$ for **(b)**. **(c)** Partial load efficiency of the selected conventional current-impressed WPT design from **(a)**, and **(d)** of the proposed current-impressed WPT design selected in **(b)**.

impressed method for multi-receiver WPT through SS, cf. **Fig. 3(b,c)**. The optimization focuses on the design of WPT through SS with two receivers with the specifications given in **Tab. I**. To this end, four core types with effective relative permeabilities ranging from 60 to 2000 are considered for the optimization, as detailed in **Tab. II**, together with core dimensions. For the optimization presented in the following, stacking multiple cores has not been considered due to the increase in weight. Besides the core type, the number of turns of the primary N_1 and the secondary N_2 windings, the switching frequency f_s, the nominal duty cycles of the active rectifier D_N, and the nominal load resistance R_{loadN} are varied to realize multiple possible design points, each with a specific nominal (maximum) power rating. The range for the optimization variables is given in **Tab. III**.

The losses in the primary and secondary windings are calculated using the method given in [12], while the core losses are calculated using Steinmetz's equation (Steinmetz's coefficients for each magnetic material are given in **Tab. IV**). The losses of the inductive components in the compensation circuit are estimated with a fixed quality factor ($Q = \omega L_f / R_f$) of 200 as a typical experience value for inductors in this inductance/current range while capacitive components are assumed to be lossless. The detailed optimization of the compensation inductor L_f will be carried out in our future work. **Fig. 7(a,b)** shows the efficiency against the nominal power per receiver for **(a)** the conventional current-impressed WPT system and **(b)**

TABLE II: The design specifications and core parameters.

Type	Part #	Material	μ_r	Dimensions
01	0076192A7	Koolmu 60	60	R58/25.6/16.2
02	C055106A2	MPP 200	200	R58/35/15
03	C055250A2	MPP 550	550	R41/23.3/15.4
04	B64290L0082	N87 Ferrite	2000	R50/30/20

TABLE III: The variation range for the optimization parameters.

Parameter	N_1	N_2	f_s	R_{loadN}
Range	[5, 30]	[5, 50]	[5 kHz, 50 kHz]	[5 Ω, 400 Ω]

TABLE IV: Steinmetz's coefficients of the selected materials [19], [20].

Steinmetz's equation[1]: $P_{\mathrm{w}} = k(f/f_0)^{\alpha}(B/B_0)^{\beta}$			
Material	k	α	β
Koolmu 60	$44.30\,\mathrm{mW/cm^3}$	1.988	1.541
MPP 200	$53.71\,\mathrm{mW/cm^3}$	2.103	1.624
MPP 550	$74.76\,\mathrm{mW/cm^3}$	2.103	1.625
N87 Ferrite	$2.793\,\mathrm{mW/g}$	1.635	2.253

[1] B_0 is 1 T, and f_0 is 1 kHz

the proposed current-impressed WPT system for different core materials. Here, the system consists of two identical receivers with the same nominal power as specified in **Tab. I**, where the input and output dc voltages are assumed to be at $72\,\mathrm{V}$ as specified in **Tab. I**, and the nominal power is varied by varying the equivalent load resistance R_{loadN}. The boundary lines shown in **Fig. 7(a,b)** correspond to the maximum attainable efficiencies with different core materials, and the scatter plots show the efficiencies and core flux densities at different design points for the best core type in each case.

For the conventional current-impressed approach (cf. **Fig. 2(b)**), a peak efficiency of around 96% is attainable for nominal power ratings ranging from $50\,\mathrm{W}$ to $700\,\mathrm{W}$ using the powder core material MPP200 ($\mu_{\mathrm{r}} = 200$). The flux density of the core can be as high as $400\,\mathrm{mT}$ for the power levels above $200\,\mathrm{W}$ (per load), which is within the saturation limits (i.e., $0.8\,\mathrm{T}$) of powder cores [19]. As discussed in **Sec. II** and shown with (6), high permeability of the core results in higher magnetic core flux density. For example, when conventional ferrite materials are used (type 4 in **Tab. II**), the flux density of the core goes above $0.8\,\mathrm{T}$ even at $100\,\mathrm{W}$ power, which is exceeding the saturation limits of ferrite (i.e., $0.45\,\mathrm{T}$). Therefore, this makes conventional ferrite materials not feasible due to core saturation and high flux density, and core losses. The efficiency for ferrite-based designs is lower than 10% and not visible in **Fig. 7(a)**. On the other hand, if the effective permeability of the core material is lower than $\mu_{\mathrm{r}} = 200$, the mutual inductance between primary and secondary windings will be reduced, which leads to significant harmonic distortion of the input current and lower efficiencies at light load. Nevertheless, using air-core coils might appear as a solution to core losses. However, very low mutual inductance and higher eddy current losses in SS limit the possibility of using air-core coils. Therefore, suitable closed core types are limited to particular core types with $\mu_{\mathrm{r}} \in [200, 300]$ for the conventional current-impressed method.

In contrast, the proposed current-impressed method results in lower magnetizing current and lower core flux densities, allowing conventional ferrite material (with, e.g., $\mu_{\mathrm{r}} = 2000$) to be used. For example, the plot in **Fig. 7(b)** shows that the proposed approach can realize efficiencies of almost $97\% - 98\%$ throughout the full range of nominal power ratings with flux densities of less than $200\,\mathrm{mT}$.

B. Performance Evaluation

Next, the target power level per load is selected to be at $100\,\mathrm{W}$ according to the application criteria, and two designs are selected from both conventional and proposed current-impress WPT systems for further evaluation (The selected design points are indicated in **Fig. 7(a,b)**.). The specification of the system parameters is given in **Tab. V**. We can see that the conventional approach results in $95.8\,\%$ efficiency at the nominal load, while the proposed method reaches $98\,\%$ efficiency at the nominal load. The efficiency improvement of the proposed approach mainly comes from lower core losses. Amplitudes of the primary and secondary currents are in a similar range for both current-impressed schemes, however, the proposed method realizes almost out of phase (phase is $-175.5°$) primary and secondary currents which compensate the magnetizing current in the core resulting in a low magnetic flux density. Note that the value of compensation inductor L_{f} is in a similar range for both systems, which results in a similar size of the compensation network, while the weight of the ferrite core is $37\,\%$ lower than the weight of the MPP200 powder core of the conventional system.

Next, the partial-load efficiencies of the two selected designs rated at $100\,\mathrm{W}$ (per load) are illustrated in **Fig. 7(c,d)**. In general, efficiency decreases at partial loads due to the constant losses in current-impressed windings. For example, the efficiency of the conventional system drops to $90\,\%$ when both loads drop their power to 50% (i.e., $50\,\mathrm{W}$), whereas the proposed system keeps the efficiency above $95\,\%$ at 50% load. The better performance of the proposed current impressed system originates from its lower flux densities in the core due to compensating primary and secondary currents. In contrast, in the conventional system, although the secondary current decreases with decreasing load power, the constant primary current dominates the core losses. Nevertheless, lower efficiency at light-load conditions is still acceptable in practical situations in terms of thermal management. Another important feature of the proposed approach is its capability to have inherent overload protection.

IV. Conclusion

This paper presents a new current-impressed wireless power transfer (WPT) scheme for efficient power transfer through stainless steel (SS) to multiple, independent receiving loads, i.e., moving tool carriages of a linear actuator (LA).

Compared to the conventional voltage-impressed method, the proposed current-impressed method allows WPT to multiple receivers without synchronization/communication. Furthermore, compared to conventional current-impressed methods, the proposed approach does not use resonant compensation on the secondary side and thus realizes lower flux densities in closed magnetic cores that are advantageously employed to minimize SS losses. This ultimately facilitates significantly higher efficiencies ($98\,\%$ vs. $96\,\%$ of a conventional current-impressed system) with low-cost ferrite core materials and better efficiency at partial load. Our future work includes the development of wirelessly powered industry-scale LAs using the proposed current-impressed WPT approach.

TABLE V: The system parameters of the optimized designs at 100 W nominal power.

Parameter	Conventional	Proposed
Core material	MPP 200	Ferrite
Frequency	25 kHz	30 kHz
Primary turns N_1	10	10
Secondary turns N_2	35	25
Primary inductance $L_1 + L_{1a} + L_{1b}$	279.2 µH	1.0 mH
Secondary inductance $L_{2\{a,b\}}$	306.2 µH	2.8 mH
Mutual inductance M	87.5 µH	1.1 mH
Primary resistance R_1	240 mΩ	266 mΩ
Compensation inductance L_f	87.5 µH	88.5 µH
Primary capacitance[1] $(-1/\omega X_{s1})$	211 nF	967 nF
Secondary capacitance $C_{2\{a,b\}}$	132 nF	–
Efficiency at nominal load	95.8 %	98 %
Core weight	190 g	120 g
Core losses	2.6 W	300 mW
Primary current (rms) at nominal load	4.7 A	3.9 A
Secondary current (rms) at nominal load	1.43 A	1.43 A
Phase between primary and secondary currents	90°	−175.5°

[1] A compensation capacitor is used in series with primary as the required series reactance X_{s1} is negative for both cases, i.e., $X_{s1} < 0$.

REFERENCES

[1] A. W. Green and J. T. Boys, "10 kHz inductively coupled power transfer - Concept and control," in *Proc. 5th Int. Conf. Power Electron. Variable-Speed Drives*, London, UK, Jan. 1994, pp. 694–699.

[2] K. W. Klontz, D. M. Divan, D. W. Novotny, and R. D. Lorenz, "Contactless power delivery system for mining applications," *IEEE Trans. Ind. Appl.*, vol. 31, no. 1, pp. 27–35, 1995.

[3] J. M. Barnard, J. A. Ferreira, and J. D. van Wyk, "Sliding transformers for linear contactless power delivery," *IEEE Trans. Ind. Electron.*, vol. 44, no. 6, pp. 774–779, 1997.

[4] S. Hasanzadeh and S. Vaez-Zadeh, "Design of a wireless power transfer system for high power moving applications," *Progress in Electromagnetics Research M*, vol. 28, pp. 258–271, 2013.

[5] G. A. Covic and J. T. Boys, "Inductive power transfer," *Proc. IEEE*, vol. 101, no. 6, pp. 1276–1289, 2013.

[6] K. Moriki, A. Kawamura, T. Shimono, T. Nozaki, K. Ikeda, J. Sato, H. Hayashiya, and H. Yamamoto, "Technological feasibility of coaxial contactless power transmission for traction power supply," in *Proc. 16th IEEE Int. Power Electron. Motion Control Conf. Expo. (EPE-PEMC)*, Antalya, Turkey, Sep. 2014, pp. 967–972.

[7] S. Li and C. C. Mi, "Wireless power transfer for electric vehicle applications," *IEEE Trans. Emerg. Sel. Topics Power Electron.*, vol. 3, no. 1, pp. 4–17, 2015.

[8] DAIFUKU Wireless Power Supply Solutions, https://www.daifuku.com/solution/list/wirelesspower/, Accessed: February 2022. .

[9] LinMot, https://linmot.com/, accessed: 01-10-2022 .

[10] S. Mirić, P. Küttel, A. Tüysüz, and J. W. Kolar, "Design and experimental analysis of a new magnetically levitated tubular linear actuator," *IEEE Transactions on Industrial Electronics*, vol. 66, no. 6, pp. 4816–4825, 2019.

[11] S. Mirić, M. Tatić, J. Huber, D. Bortis, and J. W. Kolar, ""Pushing power through walls" – Wireless power transfer through stainless steel," in *Proc. 24th Int. Conf. El. Machines and Systems (ICEMS)*, Gyeongju, Korea, Oct. 2021, pp. 743–751.

[12] S. Mirić, J. Xu, J. Huber, D. Bortis, M. Hitz, and J. W. Kolar, "Wireless power supply of moving linear actuator enclosed in stainless-steel," in *Proc. IEEE Wireless Power Week (WPW)*, Bordeaux, France, Jul. 2022.

[13] Z. Pantic, S. Bai, and S. M. Lukic, "ZCS LCC-compensated resonant inverter for inductive-power-transfer application," *IEEE Trans. Ind. Electron.*, vol. 58, no. 8, pp. 3500–3510, 2011.

[14] W. Zhang and C. C. Mi, "Compensation topologies of high-power wireless power transfer systems," *IEEE Trans. Veh. Technol.*, vol. 65, no. 6, pp. 4768–4778, 2016.

[15] N. Yan, D. Dong, and R. Burgos, "A multichannel high-frequency current link based isolated auxiliary power supply for medium-voltage applications," *IEEE Transactions on Power Electronics*, vol. 37, no. 1, pp. 674–686, 2022.

[16] J. E. Huber, J. Miniböck, and J. W. Kolar, "Generic derivation of dynamic model for half-cycle DCM series resonant converters," *IEEE Trans. Power Electron.*, vol. 33, no. 1, pp. 4–7, 2018.

[17] J. Lu, G. Zhu, D. Lin, S.-C. Wong, and J. Jiang, "Load-independent voltage and current transfer characteristics of high-order resonant network in IPT system," *IEEE Journal of Emerging and Selected Topics in Power Electronics*, vol. 7, no. 1, pp. 422–436, 2019.

[18] K. Colak, E. Asa, M. Bojarski, D. Czarkowski, and O. C. Onar, "A novel phase-shift control of semibridgeless active rectifier for wireless power transfer," *IEEE Trans. Power Electron.*, vol. 30, no. 11, pp. 6288–6297, 2015.

[19] "MPP cores," https://www.mag-inc.com/Products/Powder-Cores/MPP-Cores, accessed: 2022-08-01.

[20] "Core loss data sheet MnZn ferrite N87," https://www.tdk-electronics.tdk.com, accessed: 2022-08-01.